Re-visiting the atmospheric corona

Philip Laven

9 Russells Crescent, Horley, Surrey RH6 7DJ, UK (philip@philiplaven.com)

Received 2 September 2014; accepted 30 September 2014;
posted 16 October 2014 (Doc. ID 222057); published 14 November 2014

The atmospheric corona is a well-known diffraction phenomenon, typically seen as colored rings surrounding the Sun or Moon. In many respects, Fraunhofer diffraction provides a good explanation of the corona. As the angular sizes of the corona's rings are inversely proportional to the radius, r, of the spherical particles causing the corona, it should be easy to estimate the particle size from observations and photographs. Noting that some of the techniques commonly used for particle sizing based on diffraction theory can give misleading results for coronas caused by the scattering of sunlight, this paper uses Mie theory simulations to demonstrate that the inner 3 red rings of the corona have angular radii of $\theta \approx 16/r, 31/r$, and $47/r$, when θ is measured in degrees and r is measured in μm. © 2014 Optical Society of America

OCIS codes: (010.1290) Atmospheric optics; (290.1310) Atmospheric scattering; (290.2558) Forward scattering.

http://dx.doi.org/10.1364/AO.54.000B46

1. Introduction

The corona typically appears as a series of colored concentric rings around a partially cloud-covered Sun or Moon. This diffraction phenomenon should not be confused with the solar corona (which is caused by plasma being ejected from the surface of the Sun). Diffraction by a spherical particle, such as a droplet of water, can be modeled by Fraunhofer diffraction,

$$I(\theta) \propto \left[x \frac{[1+\cos\theta]}{2} \frac{(J_1[x \sin\theta])}{[x \sin\theta]} \right]^2, \qquad (1)$$

where

$I(\theta)$ is the intensity of the scattered field at scattering angle θ;
$x = 2\pi r/\lambda$;
r is the radius of the spherical particle;
λ is the wavelength of the light;
J_1 is the first-order Bessel function.

Figure 1 shows the results of calculations based on Eq. (1), assuming a spherical droplet of water with $r = 10$ μm for red, green, and blue monochromatic light. The rings of the corona correspond to local maxima in the last term of Eq. (1), with the first 4 occurring when $x \sin\theta = 5.136$, 8.417, 11.62, and 14.796.

As θ is small, these local maxima occur at $\theta \approx \sin\theta = 0.8174\lambda/r$, $1.3396\lambda/r$, $1.8494\lambda/r$, and $2.3548\lambda/r$. If θ is expressed in degrees and r is measured in μm, the inner rings of the corona for red light ($\lambda = 0.65$ μm) can be defined by $\theta_1 = 30.44/r$, $\theta_2 = 49.89/r$, $\theta_3 = 68.87/r$, and $\theta_4 = 87.7/r$.

Table 1 lists the locations of the corona's rings for monochromatic blue, green, and red light. Examination of individual rows of Table 1 suggests that the rings of a given order (e.g., the second ring denoted by θ_2) follow a strict sequence with a blue inner ring, followed by a green ring, and then a red outer ring. However, comparison of different rows in Table 1 shows considerable overlap between rings of different orders: for example, the third-order red ring at $\theta_3 = 68.87/r$ coincides with the fourth-order green ring at $\theta_4 = 68.81/r$, as can be seen in Fig. 1. Such overlaps suggest that the colors of the atmospheric corona cannot be spectrally pure.

1559-128X/15/040B46-08$15.00/0
© 2015 Optical Society of America

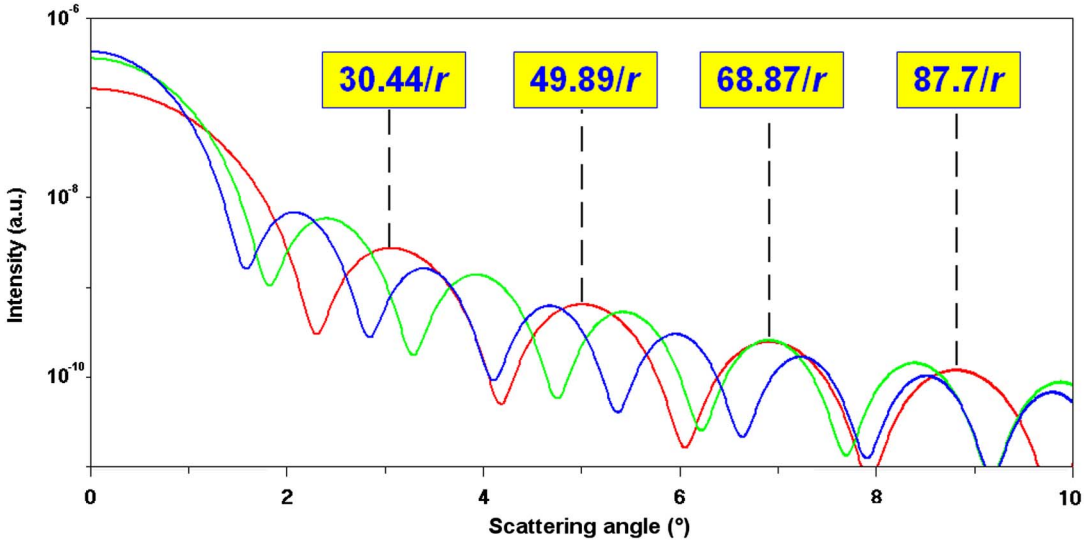

Fig. 1. Diffraction calculations for a spherical water droplet of radius, $r = 10$ μm, showing the scattered intensity as a function of scattering angle, θ, for three wavelengths (red = 0.65 μm, green = 0.51 μm, blue = 0.44 μm). The relative intensities of the three wavelengths have been adjusted to approximate the Sun's spectrum. The calculations take into account the apparent diameter of the Sun (0.5°). The vertical dashed lines mark the local maxima for red light as a function of r [as derived from Eq. (1)].

Table 1. Angle θ of the Corona's Rings for Scattering of Monochromatic Light by a Spherical Particle of Radius, r

	Blue	Green	Red
Maximum	$\lambda = 0.44$ μm	$\lambda = 0.51$ μm	$\lambda = 0.65$ μm
θ_1	$20.61/r$	$23.88/r$	$30.44/r$
θ_2	$33.77/r$	$39.15/r$	$49.89/r$
θ_3	$46.62/r$	$54.04/r$	$68.87/r$
θ_4	$59.37/r$	$68.81/r$	$87.70/r$
θ_5	$72.06/r$	$83.52/r$	$106.45/r$
θ_6	$84.73/r$	$98.21/r$	$125.17/r$

2. Simulations of Coronas

Figure 2 compares simulations of the coronas for monochromatic light with the atmospheric corona caused by the scattering of sunlight. These simulations have been calculated using Eq. (1). In the case of the sunlight corona, the simulation assumed 100 equally-spaced wavelengths between 0.38 and 0.7 μm. Note that the monochromatic coronas have many more rings than the sunlight corona.

All of the simulations in Fig. 2 assume scattering from a spherical droplet of water with $r = 10$ μm (which is typical of corona-causing clouds), but it is not obvious how the colored rings of the sunlight corona are related to the monochromatic coronas. For example, do the calculated maxima for monochromatic red light coincide with the red rings in the corona caused by sunlight?

As the outer rings of the corona are so much weaker than the Sun, it is imperative to avoid damage to human eyes caused by looking at the sunlight corona. Although observers can use the shadow of a building to avoid direct sunlight, the moonlight corona is more familiar because our eyes can withstand the glare of the Moon. Nevertheless, it is

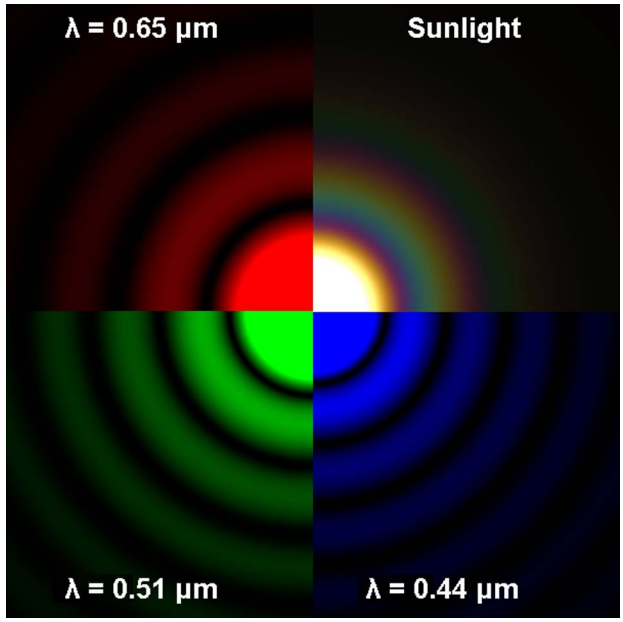

Fig. 2. Simulations of coronas caused by the scattering of monochromatic light and sunlight by a water droplet of radius, $r = 10$ μm. In each case, the brightness has been increased by a factor of 10 to show more detail in the outer rings, but results in "overexposure" of the central zone of the coronas.

impossible to reproduce the full dynamic range of any type of corona in a printed document or on a standard computer display. The horizontal bars above the graph in Fig. 3 show three representations of a simulation of the corona. The brightness of the lowest bar has been normalized so that the brightest part of the simulation (i.e., the central zone of the corona at $\theta = 0°$) is reproduced with at least one of the RGB values equal to the maximum value of

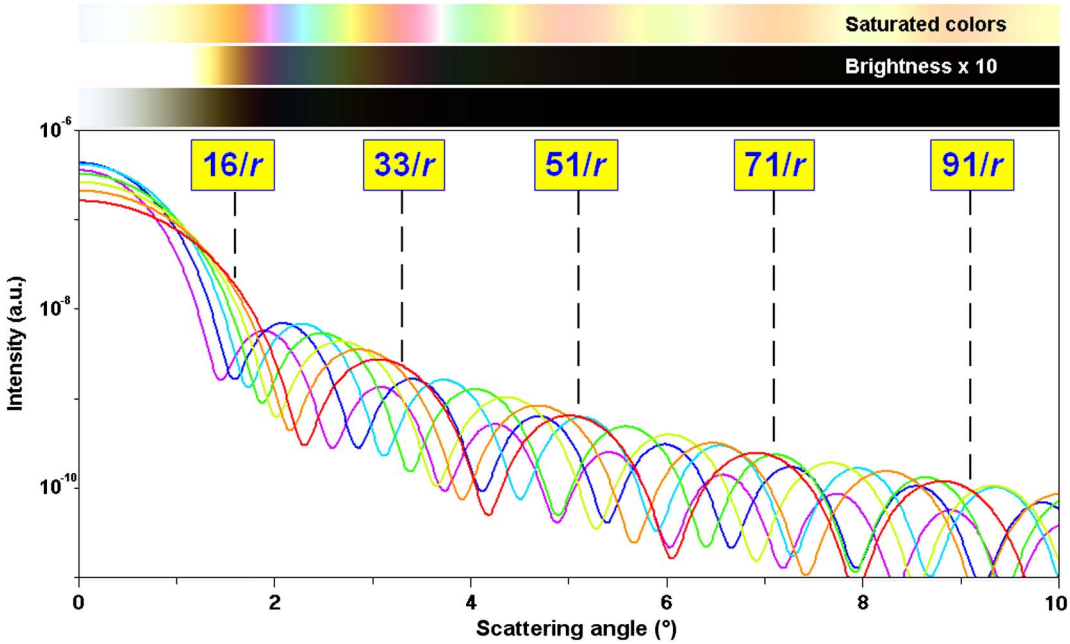

Fig. 3. Diffraction calculations for the corona caused by scattering of sunlight by a spherical water droplet of radius, $r = 10$ μm.

255. The middle bar has its brightness increased by an arbitrary factor of 10 to reveal the rings of the corona, but this is achieved by overexposing the central zone. Finally, another technique to show the rings of the corona has been used in the top horizontal bar: instead of simulations reproducing the correct relative intensities of the scattered light, the top bar shows the "saturated colors" of the corona. In other words, information about the brightness of the corona has been removed, leaving only colors that have been normalized so that at least one of the RGB values has the maximum value of 255; hence, the term "saturated color."

The results in Fig. 3 show that red (or reddish) rings occur at $\theta \approx 16/r$, $33/r$, $51/r$, $71/r$, and $91/r$, whereas the monochromatic results in Fig. 1 suggested that red rings should appear at $\theta \approx 30.44/r$, $49.89/r$, $68.87/r$, and $87.7/r$. Note that this simulation of the sunlight corona shows an additional red ring at $16/r$, which does not correspond to a local maximum in the calculations for monochromatic red light. Despite this major discrepancy, the other

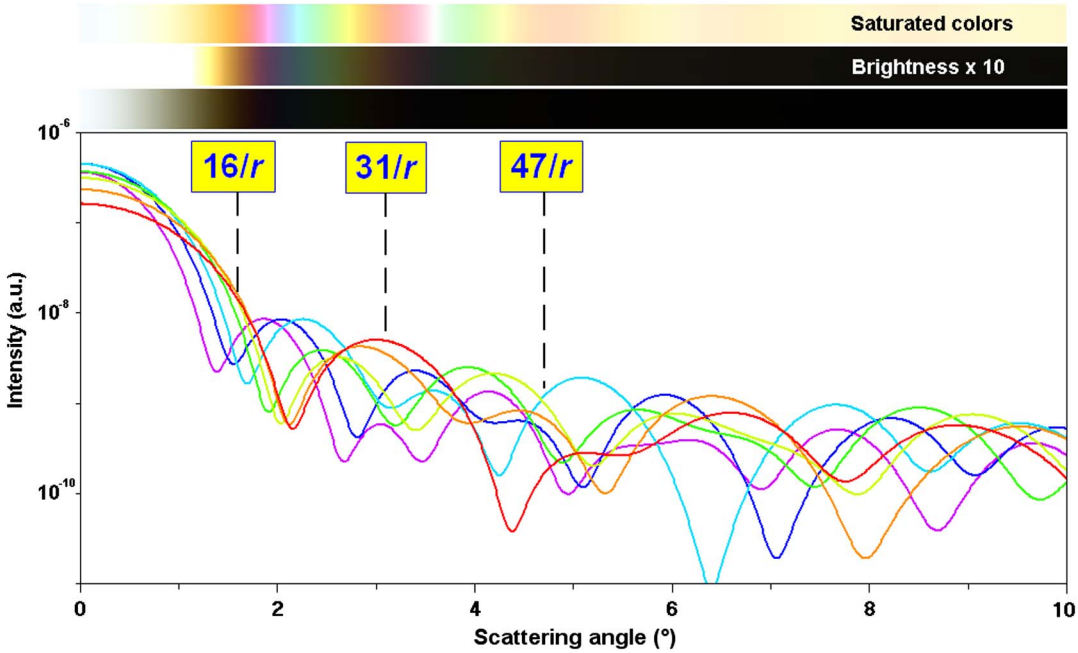

Fig. 4. Same as Fig. 3 but using Mie theory.

Fig. 5. Image of a three-ringed lunar corona. The arrow shows the location of the third red ring. © Lauri Kangas.

Table 2. Angle, θ, of the Corona's Red Rings for Scattering of Sunlight by a Spherical Particle of Radius, r

Monochromatic Light	Sunlight	
$\lambda = 0.65$ μm	Diffraction	Mie
—	$16/r$	$16/r$
$30.44/r$	$33/r$	$31/r$
$49.89/r$	$51/r$	$47/r$
$68.87/r$	$71/r$	—
$87.70/r$	$91/r$	—

values derived from Fig. 1 are roughly similar to the remaining red rings in Fig. 3.

As diffraction calculations are only an approximation, it is relevant to compare the above results with those obtained using Mie theory, as in Fig. 4, which shows red rings at $\theta \approx 16/r$, $31/r$, and $47/r$. Note that only three red rings are visible in Fig. 4 despite the use of "saturated colors" to emphasize the visibility of the colored rings. Although many rings are visible on monochromatic coronas under laboratory conditions (as illustrated by the simulations in Fig. 2), sunlight coronas have fewer rings.

Furthermore, Fig. 4 shows that the corona for $r = 10$ μm exhibits colors that are essentially uniform when $\theta > 6°$. This implies that, even under ideal circumstances with droplets of uniform size, it is unlikely that coronas will have more than three rings. Figure 5 shows a lunar corona in which the central portion has been overexposed to permit the corona's rings to be seen more clearly. Two red rings can easily be seen in Fig. 5, but the third red ring is barely visible.

Table 2 summarizes the location of the red rings of the sunlight corona. It is important to stress that the red ring at $\theta \approx 16/r$ is not caused by discrepancies between diffraction theory and Mie theory. Comparing the simulations in Fig. 6, there are some minor differences in the position and visibility of the corona's outer rings, but both calculation methods produce a red ring at $\theta \approx 16/r$.

What causes this "extra" red ring? The graphs in Figs. 3 and 4 show that the forward-scattering lobe centered on $\theta = 0°$ is wider for red light than for violet light. Consequently, the graphs show that scattering in the vicinity of $\theta = 16/r$ is dominated by red light, thus causing the unexpected red ring. A related phenomenon is the aureole, which consists of a circular white zone surrounded by a reddish edge. The simulations in Fig. 6 assume that all of the water droplets are exactly the same size (i.e., monodisperse with $r = 10$ μm). As this assumption is unlikely to be valid in practice, Fig. 7 shows simulations of scattering from water droplets having a log–normal distribution with a median value of $r = 10$ μm and the specified standard deviation, σ. For large values of σ, only the aureole is visible suggesting that the aureole is simply a corona in which the outer rings are not visible.

It is fascinating to note that many authors seem to be unaware that the inner ring of the corona is red. For example, Brooks [1] says, "*As the wave fronts of the light of shorter wavelengths, e.g., blue, are least diffracted in passing through a dusty or cloudy medium, the color seen nearest the Sun or Moon is bluish, and is followed in succession by green, yellow, orange, and red*. Similarly, Humphreys writes [2] "*Thin clouds of water droplets also produce beautiful colored rings about the Sun and Moon, but usually*

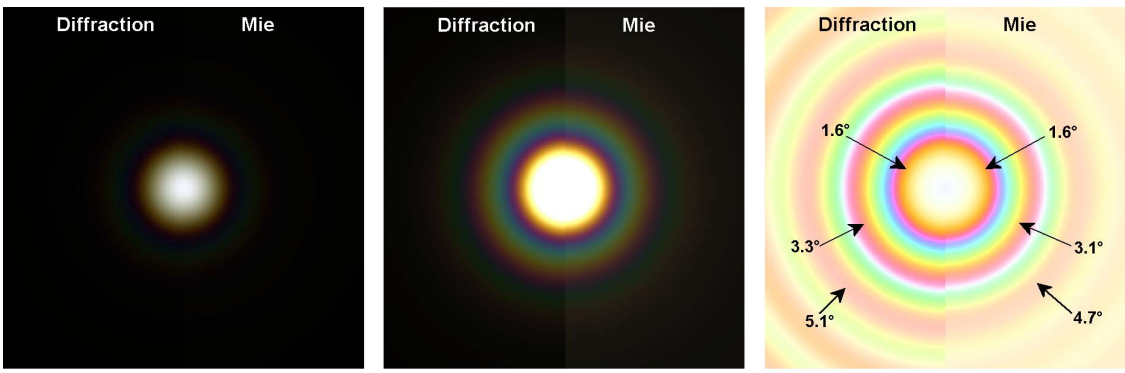

Fig. 6. Comparison of simulations using diffraction theory and Mie theory. Diagram (a) shows normal brightness, (b) shows the effect of increasing the brightness of the simulation by a factor of 10, and (c) shows saturated colors.

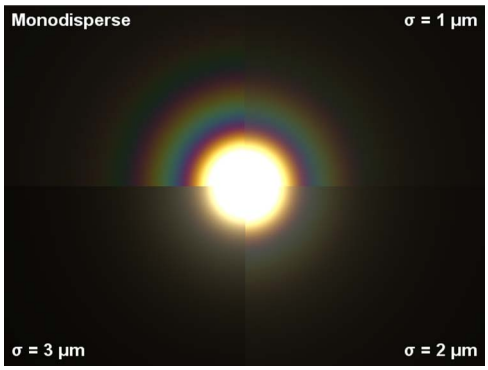

Fig. 7. Simulations of coronas caused by scattering of sunlight by spherical water droplets with log–normal size distributions (median radius, $r = 10$ μm, with standard deviation σ).

much smaller than the circles formed by refraction through snow crystals, and with their colors in reverse order, that is, with the red farthest from the source of light, instead of nearest to it." Lynch and Livingston write [3] "*… coronae colors go from white in the middle (an aureole) to blue, green, yellow, and red and this series repeats outward for each successive ring.*"

Minnaert is one of the few authors supporting the idea of a red inner ring. He identifies four groups, which he describes as: [4] "*I. Aureole (bluish)–white–(yellowish)–brown-red; II Blue–green–(yellow)–red; III. Blue–green–red; IV. Blue–green–red.*" Minnaert's separation of the corona into an aureole surrounded by sets of coronal rings is intriguing because the aureole corresponds to the forward-scattering lobe centered on $\theta = 0°$, while the rings correspond to local maxima in the diffraction pattern.

The assertions that the inner ring of the corona is blue are probably due to the authors' familiarity with diffraction theory, which, as highlighted in Table 1, predicts smaller blue rings inside larger red rings. Having carefully observed many coronas, I have yet to see a corona that does not have a red inner ring. Of course, my personal belief that the inner ring of the corona is red could be the result of looking at too many simulations!

3. Particle Sizing

Attempts at particle sizing based on the radius of the rings must take into account the extra red ring at $\theta \approx 16/r$. If this ring is ignored, the particle radius, r, will be seriously overestimated.

Given the common belief that the inner red ring of the corona occurs at $\theta = 30.44/r$, it is not surprising that many authors (including the author of this paper) have made mistakes when estimating particle sizes. As an example, an analysis of a photograph of a corona is given in [5] in which three rings are defined as shown in the left side of Table 3, resulting in an estimated mean value of $r = 7.25$ μm. In addition to missing the red ring at $\theta \approx 16/r$, the blue ring at $\theta = 5.23°$ is incorrectly identified as the second-order blue ring when it is actually the first-order blue ring. The right side of Table 3 uses equations derived from Fig. 4 to give a mean value of $r = 4.16$ μm.

The first four local minima in Eq. (1) occur when $x \sin\theta = 3.832$, 7.016, 10.17, and 13.32. As θ is small, these minima occur at $\theta \approx \sin\theta = 1.2197\lambda/(2r)$, $2.2331\lambda/(2r)$, $3.2383\lambda/(2r)$, and $4.2411\lambda/(2r)$, leading to the widely-used approximation for the location, θ_n, of the nth minima,

$$\theta_n \approx (n + 0.22)\lambda/(2r). \tag{2}$$

It has been suggested that Eq. (2) can be used to determine the location of the red rings by selecting an appropriate wavelength, $\lambda_0 = \lambda$. It is not immediately obvious how to select λ_0, but $\lambda_0 = 0.57$ μm has been widely used for many years [6,7]. More recently, $\lambda_0 = 0.49$ μm has been shown to give more accurate results [8,9]. van de Hulst offers some guidance on this issue [10] "*… the first minimum in the diffraction pattern for green light gives the hue of its complementary color, red. This is in analogy with an old theory for the colors of the diffraction corona, in which it has been customary to interpret the outer edge of the first red zone as the first minimum for "white light" with* $\lambda = 0.56$ μm."

It is worth exploring this concept of complementary colors. Our visual perception of the colors of the corona is the result of stimulus by a continuous spectrum of scattered light rather than light of a single wavelength. Hence, we need to understand how light of different wavelengths affects, for example, the perceived redness of various parts of the corona. Figure 8 shows a CIE diagram in which the pure spectral colors are arranged along a curved arc. As we are interested in red rings, a dominant wavelength of $\lambda = 0.65$ μm has been highlighted. If the line from $\lambda = 0.65$ μm to the white point is extended, it reaches the spectral locus at its complementary wavelength of $\lambda = 0.486$ μm. Moving from the white point along the red line toward $\lambda = 0.65$ μm corresponds to increasing redness. Similarly, moving along the blue line from $\lambda = 0.486$ μm toward the white point corresponds to decreasing blueness.

Table 3. Calculations of Particle Radius, *r*

	Data from Table 1 of [5]		Revised Calculations	
θ	Designation	Equation	Designation	Equation
3.66°	1st-order red ($\lambda = 0.63$ μm)	$r = 29.51/\theta = 8.07$ μm	First-order red	$r = 16/\theta = 4.37$ μm
5.23°	2nd-order blue ($\lambda = 0.49$ μm)	$r = 37.61/\theta = 7.19$ μm	First-order blue	$r = 20.6/\theta = 3.94$ μm
7.44°	2nd-order red ($\lambda = 0.63$ μm)	$r = 48.35/\theta = 6.5$ μm	Second-order red	$r = 31/\theta = 4.17$ μm

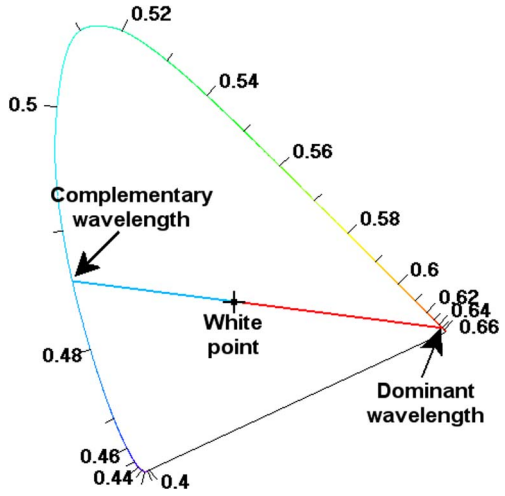

Fig. 8. Dominant and complementary wavelengths.

Table 4. Angle, θ, of the Corona's Red Rings for Scattering of Sunlight by a Spherical Particle of Radius, r

	Diffraction Minima [using Eq. (2)]	
Mie	$\lambda_0 = 0.486$ μm	$\lambda_0 = 0.57$ μm
$16/r$	$16.98/r$	$19.91/r$
$31/r$	$31.09/r$	$36.47/r$
$47/r$	$45.09/r$	$52.88/r$

and, crucially, to increasing redness. Hence, in a continuous spectrum, reducing the intensity of light with $\lambda = 0.486$ μm will cause the remaining light to appear more red. Figure 8 suggests that $\lambda_0 = 0.486$ μm should be used in Eq. (2) to predict the location of the red rings.

Table 4 compares the locations of the red rings calculated using Mie theory and by using Eq. (2) with two different values of λ_0. The results obtained with $\lambda_0 = 0.486$ μm are fairly similar to the Mie theory results, thus confirming the previously reported preference for $\lambda_0 = 0.49$ μm. In practice, no single value of λ_0 would give a perfect match to the Mie theory results shown in Table 4: $\theta = 16/r$ would require $\lambda_0 = 0.4579$ μm; $\theta = 31/r$ would require $\lambda_0 = 0.4845$ μm, and $\theta = 47/r$ would require $\lambda_0 = 0.5066$ μm. This raises the issue of why we should be interested in the indirect calculations based on diffraction theory. In the past, diffraction theory was attractive because it was simple (assuming access to tables of Bessel functions) whereas Mie theory involved difficult and time-consuming computations. As calculations using Mie theory are no longer prohibitively complicated, it is obviously better to rely on Mie theory.

4. Effect of Particle Size

As diffraction theory based on Eq. (1) indicates that the size of the corona's rings is inversely proportional to particle radius, r, this paper has so far made the assumption that the red rings can be defined in terms of r. This assumption is tested in Fig. 9, which uses Lee diagrams [11] to compare simulations obtained by diffraction theory and by Mie theory. As shown by Fig. 9(a), the diffraction model produces uniform colored rings in which the scattering angle, θ, is inversely proportional to r. Figure 9(b) shows

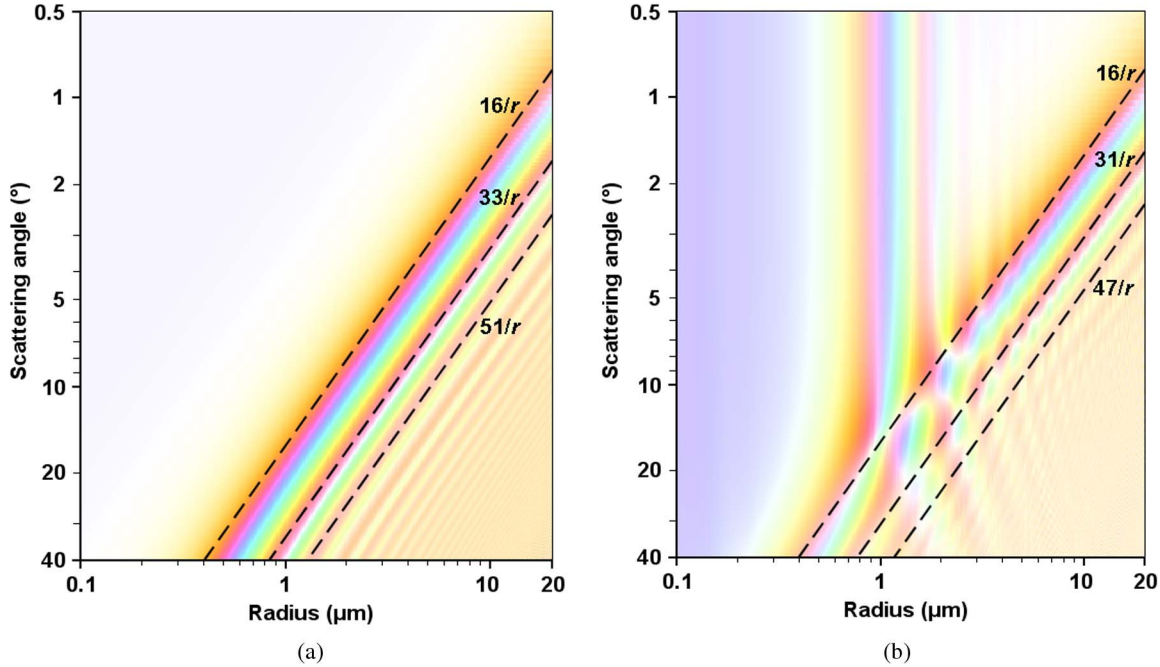

Fig. 9. Lee diagrams showing how the saturated colors of the corona vary with radius, r, of a spherical droplet of water. Diagram (a) shows the result of calculations using diffraction theory, while (b) shows the result of calculations using Mie theory. As these diagrams have logarithmic axes for scattering angle, θ, and for radius, r, the dashed straight lines indicate the theoretical inversely proportional relationship between θ and r.

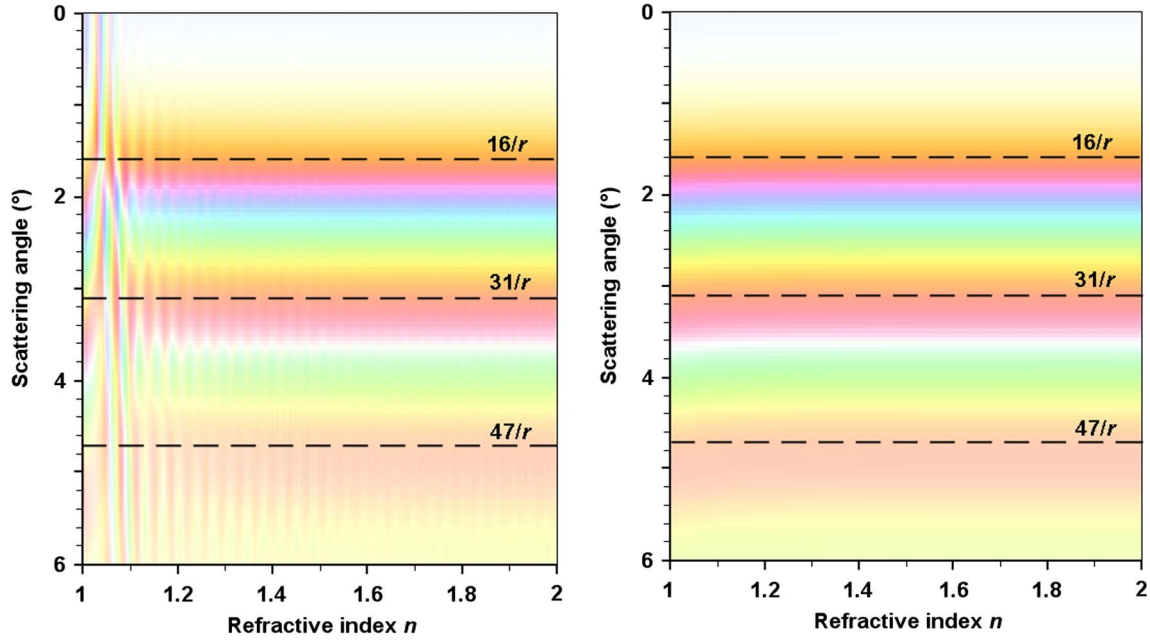

Fig. 10. Diagram showing how the saturated colors of the corona vary with refractive index, $n + ik$, calculated using Mie theory for scattering of sunlight by a spherical particle of radius, $r = 10$ μm. Diagram (a) shows results as a function of n for nonabsorbing particles (i.e., $k = 0$), while (b) shows results for absorbing particles (i.e., $k = 0.01$).

that Mie theory gives similar results to diffraction theory when $r > 3$ μm [12,13]. However, when $0.5\ \mu\text{m} < r < 3\ \mu\text{m}$ and $\theta < 10°$, the Mie results show that the rings of the corona are replaced by colors that vary with r but are almost independent of θ. Furthermore, very complicated patterns of color appear at larger values of θ due to "anomalous diffraction," which is the result of interference between diffracted light and light that has been transmitted through the spherical droplet [10,13]. For even smaller particles, such as $r = 0.1$ μm, Fig. 9(b) shows a blue color that is due to Rayleigh scattering.

5. Effect of Refractive Index

All of the calculations presented so far in this paper have assumed that coronas are caused by the scattering of sunlight by spherical droplets of water. Although diffraction theory as stated in Eq. (1) does not take any account of refractive index, all of the Mie theory results have been based on the refractive index, $n + ik$, of water, which varies between $n = 1.3445$ at $\lambda = 0.4$ μm and $n = 1.3314$ at $\lambda = 0.7$ μm [14], with $k \approx 10^{-8}$. However, the resulting simulations are identical if the Mie calculations are repeated using an arbitrary value of n (e.g., $n = 1.3333$) that does not vary with λ.

The dependence on refractive index is explored further in Fig. 10, which plots the saturated colors of the corona for a spherical particle of radius, $r = 10$ μm, as a function of the real part of the refractive index, n, of the particle, assuming that n does not vary with λ. Figure 10(a) shows results for a nonabsorbing particle (i.e., the imaginary part of the refractive index, $k = 0$) whereas Fig. 10(b) shows results for a very absorbing particle (i.e., $k = 0.01$). These diagrams show that the corona is essentially independent of n for nonabsorbing particles when $1.2 < n < 2$ and for absorbing particles when $1 < n < 2$. The cyclic variations shown in Fig. 10(a) when $1 < n < 1.2$ are due to anomalous diffraction, as previously noted in reference to Fig. 9(b). Such variations do not appear in Fig. 10(b) because the light transmitted through the particle is strongly attenuated, leaving only the diffracted component. Comparisons of Figs. 10(a) and 10(b) indicate that the corona's appearance is also effectively independent of k, at least for particles with $r = 10$ μm.

The corona's independence of refractive index emphasizes that the nature of the scattering particles (e.g., water, ice, pollen, etc.) is less important than the size and shape of the scattering particles.

6. Conclusions

The atmospheric corona is caused by the scattering of sunlight by spherical droplets of water. When the droplet radius, $r > 3$ μm, Fraunhofer diffraction provides a good explanation of the corona, with only minor differences compared with calculations using Mie theory.

As the angular radius of the corona's circular rings is inversely proportional to r, images of the corona can easily be used to determine the value of r. However, incorrect assumptions have frequently been made about the connection between the diffraction patterns for monochromatic light and the colored rings of the corona caused by the scattering of sunlight.

One "rule of thumb" is that the red rings in the sunlight corona correspond to the maxima in the diffraction patterns for red light. Although this is a good approximation for the second and third red rings, the sunlight corona has an extra inner red ring that is not predicted by diffraction theory. Consequently, use of diffraction theory can result in particle sizes being overestimated by a factor of about 1.9.

Another widely-used "rule of thumb" is that the red rings in the sunlight corona correspond to minima in the diffraction pattern at another wavelength, $\lambda_0 = 0.57$ μm. In recent years, $\lambda_0 = 0.49$ μm has become more favored. This technique overcomes the problem of the extra red ring, even if the choice of λ_0 might seem somewhat arbitrary. This paper suggests that $\lambda_0 = 0.486$ μm would be a logical choice because this wavelength is a complementary color to red.

There is no doubt that Fraunhofer diffraction is appealing because of its mathematical simplicity compared with Mie theory, which is rigorous but opaque in its meaning. Nevertheless, particle sizing based on simple formulas derived from the diffraction patterns for monochromatic light can yield seriously misleading results. It is therefore recommended that particle sizing should be based on Mie theory simulations of the scattering of sunlight, which show that the three inner red rings of the corona have angular radii of $\theta_1 \approx 16/r$, $\theta_2 \approx 31/r$, and $\theta_3 \approx 47/r$, when θ is measured in degrees and r is measured in μm.

References

1. C. F. Brooks, "Coronas and iridescent clouds," Mon. Weather Rev. **53**, 49–58 (1925).
2. W. J. Humphreys, "Fogs and clouds," J. Franklin Inst. **193**, 327–384 (1922).
3. D. K. Lynch and W. Livingston, *Color and Light in Nature* (Cambridge University, 2001), Sect. 4.13.
4. M. Minnaert, *The Nature of Light and Colour in the Open Air* (Dover, 1954), p. 214.
5. J. A. Shaw and N. J. Pust, "Icy wave-cloud lunar corona and cirrus iridescence," Appl. Opt. **50**, F6–F11 (2011).
6. G. C. Simpson, "Corona and iridescent clouds," Q. J. R. Meteorol. Soc. **38**, 291–302 (1912).
7. W. J. Humphreys, *Physics of the Air* (McGraw-Hill, 1929), Chap. 6.
8. J. Lock and L. Yang, "Mie theory model of the corona," Appl. Opt. **30**, 3408–3414 (1991).
9. K. Sassen, "Elliptical pollen corona from North American boreal paper birch trees (Betula papyrifera): strong fall orientations for near-spherical particles," Appl. Opt. **50**, F1–F5 (2011).
10. H. C. van de Hulst, *Light Scattering by Small Particles*, reprint of 1957 Wiley ed. (Dover, 1981).
11. R. L. Lee, "Mie theory, Airy theory, and the natural rainbow," Appl. Opt. **37**, 1506–1519 (1998).
12. S. D. Gedzelman and J. A. Lock, "Simulating coronas in color," Appl. Opt. **42**, 497–504 (2003).
13. P. Laven, "Simulation of rainbows, coronas and glories using Mie theory and the Debye series," J. Quant. Spectrosc. Radiat. Transfer **89**, 257–269 (2004).
14. International Association for the Properties of Water, and Steam, "Release on the refractive index of ordinary water substance as a function of wavelength, temperature and pressure" (1997), http://www.iapws.org/relguide/rindex.pdf.